Microfluid Nanofluid (2008) 5:383–393
DOI 10.1007/s10404-007-0255-3

RESEARCH PAPER

High-current density DC magenetohydrodynamics micropump with bubble isolation and release system

Bao Nguyen · Samuel Kinde Kassegne

Received: 8 October 2007 / Accepted: 8 December 2007 / Published online: 8 January 2008

Abstract One of the major challenges for integrated Lab-on-a-Chip (LOC) systems is the precise control of fluid flow in a micro-flow cell. Magnetohydrodynamics (MHD) micropumps which contain no moving parts and capable of generating a continuous flow in any ionic fluid offer an ideal solution for biological applications. MHD micropumping has been demonstrated by using both AC and direct current (DC) currents by a number of researchers with varying degrees of success. However, current MHD designs based on DC do not meet the flow rate requirements for fully automated LOC applications (>100 μl/min). In this research, we introduce a novel DC-based MHD micropump which effectively increases flow rate by limiting the effects of electrolysis generated bubbles at the electrode–electrolyte interface through isolation and a mechanism for their release. Gas bubbles, particularly, hydrogen generated by high current density at the electrodes are the main culprit in low experimental flow rate compared with theoretical values. These tiny bubbles coalesce in the flow channel thus obstructing the flow of fluid. Since hydrolysis is inevitable with DC excitation, compartmentalized electrode channels with bubble isolating and coalescence retarding mechanisms and bubble release systems are implemented to prevent the coalescence of these bubbles and minimize their effects on flow rate. In this novel design called bubble isolation and release system, flow rate of up to 325 μl/min is achieved using 1 M NaCl solution in DC mode with potentials of 5 V and current density of about 5,000 A/m^2 for a main channel of 800 μm × 800 μm cross-section and 6.4 mm length.

Keywords DC current · Lab-on-a-chip · LOC · MHD · Microfluidics · Micropumping · Electrolysis · BioMEMS

1 Introduction

Magnetohydrodynamics (MHD) micropumps operate by virtue of the body force generated by interaction between electrical current and a perpendicular magnetic field passing through an electrolytic solution. This body force, called Lorentz force, moves the charged ions and hence the bulk fluid perpendicular to the plane formed by the orthogonal magnetic and electric fields (Fig. 1a). This concept was originally described in 1942 by Alfven (1942) as electromagnetic hydrodynamic wave.

The main reasons for the significant interest in MHD micropumps for microfluidic applications are the absence of moving parts, simple fabrication processes, lower actuation voltages, reduced risk of clogging and damage to molecular materials, reduced risk of mechanical fatigue and a continuous fluid flow (Patel and Kassegne 2007). At the macro-scale, MHD pumps are used in fusion reactors, power plants, liquid metal processing, propulsion engines, and many other applications (Strachan et al. 1987; Sutton and Sherman 1965). At the micro-scale, on the other hand, MHD pumps have found use in pumping biological fluid. However, for microfluidic applications, few phenomena that are negligible at the macro-level, such as electroosmosis, Joule heating and bubble formation, emerge as major obstacles at the micro-level.

B. Nguyen · S. K. Kassegne (✉)
MEMS Research Lab, Department of Mechanical Engineering, College of Engineering, San Diego State University, 5500 Campanile Drive, San Diego, CA 92182-1323, USA
e-mail: kassegne@mail.sdsu.edu

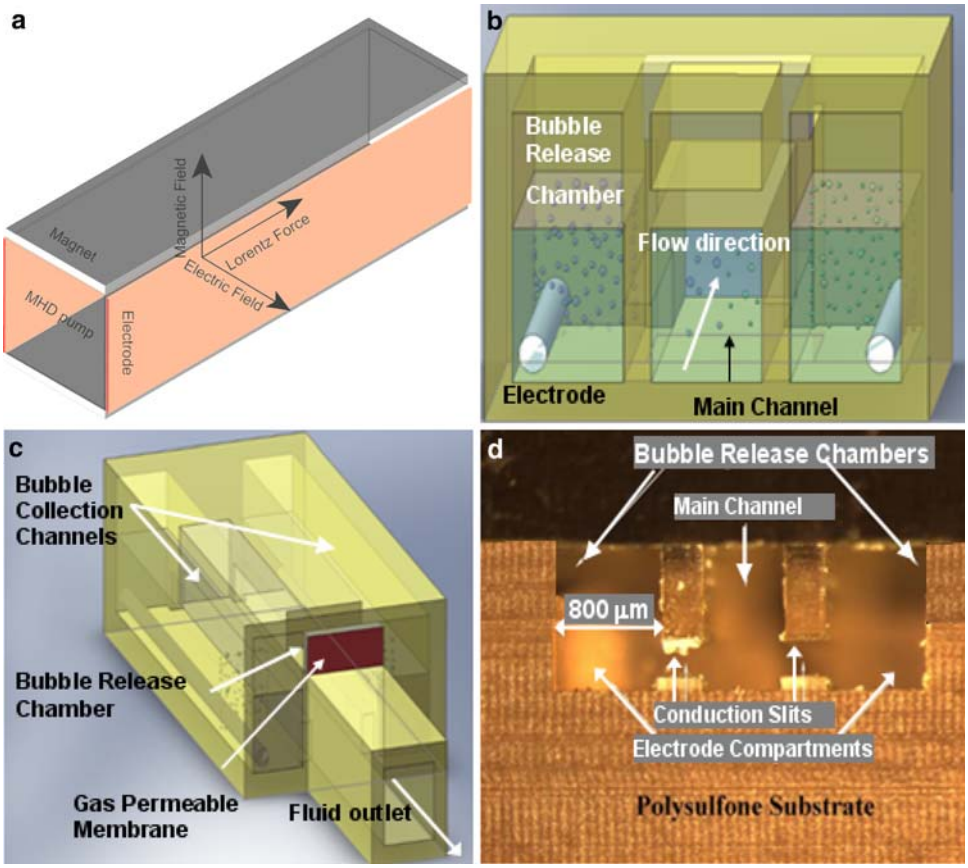

Fig. 1 **a** Typical schematic configuration of MHD micropump with a rectangular cross-section. **b** Front view of BIRS micropump with bubble isolation, collection (air vent) and release chambers. Bubbles are generated in the side channels (800 µm wide) where they develop positive pressure. This chamber is connected to a bubble collection channel or air vent (6.4 mm long) that in turn is connected to a bubble release chamber that is at atmospheric pressure. **c** Posterior view of BIRS micropump showing the bubble release system (2.4 mm wide and 2 mm long) and hermetic sealing at the back of the air vent using gas permeable membrane. **d** Cross-section of manufactured BIRS micropump

MHD micropump feasibility has been demonstrated by using both AC and direct current (DC) current by Lemoff and Lee (2000), Jang and Lee (2000), Bao and Harrison (2003), Jeong and Yang (2000), Homsy et al. (2005) with varying success. However, current DC MHD designs do not satisfy the flow rate requirement for fully automated Lab on Chip (LOC) applications. Patel and Kassegne (2007) provide a perspective to the range of MHD micropumps developed so far. The sizes of the micropumps vary from 2 mm deep (Wang et al. 2004) to 10 µm by 10 µm (Bao and Harrison 2003). Current and magnetic flux densities vary from a maximum of 4,000 A/m^2 by Homsy et al. (2005) and 2.2 Tesla (T) by Heng et al. (1999) to 1.8 mA (Jang and Lee 2000) and 420 mT (Homsy et al. 2005). The flow rates vary from 6,010 µl/min for the nozzle/diffuser micropump of Heng et al. (1999) to 0.002 pl/min of Bao and Harrison (2003). Both AC and DC sources have been used (Bendib and Français 1999; Heng et al. 2000; Heschel et al. 1997; Huang et al. 1999, 2000). With regard to micromachining processes, bulk micromachining of silicon using LIGA, inductively coupled plasma reactive ion etching (ICP-RIE), and anisotropic wet etching together with soft lithography have been used.

The first attempt in using high-current density MHD micropumps and minimizing the effect of bubbling was carried out by Homsy et al. (2005) who achieved pumping at a high current density of 4,000 A/m^2. The effect of bubbles was reduced through an external channel system located on the two longitudinal sides. The maximum flow rate they reported was only 0.5 µl/min for a channel of 75 µm × 150 µm cross-section. Further, their work does not explicitly address the actual physical release system for the bubbles, which for hermetically sealed LOC systems is an important design constraint.

In this research, we introduce novelty by placing the electrodes along the pumping length in supplementary bubble isolation and electrode channels and introducing a bubble release system on top of the flow cell which collects these bubbles and releases them to the outside environment at atmospheric pressure conditions (see Fig. 1b–d). The full-length electrodes embedded in the peripheral channels provide electric field to generate Lorentz force. Narrow gaps at the bottom of the walls between the three chambers ensure electrical continuity through out the whole pump. In this manner, the electric field distribution, hence the Lorentz force, could be manipulated by varying the geometry of the gaps. Further, the wall above the slits act as guiding track for electrolyzed bubbles to escape to an air chamber above the fluid level. The electric field and, hence, the Lorentz force is maximized due to this geometric constriction between the two channels. Further, this configuration provides a guided bubble release system to

the outside as shown in Fig. 1. For fast development time, MHD micropumps presented here are fabricated from polysulfone using computer numerical control (CNC) techniques rather than conventional silicon or glass micromachining. Compartmentalized electrode channels in conjunction with air traps allows for a maximum flow rate 325 µl/min in DC mode for 1 M NaCl solution at 5 V excitation. This design could also accommodate AC mode but it is beyond the scope of this research. The main design that is presented in this research, hereafter known as, bubble isolation and release system (BIRS) has the main distinct features of compartmentalization for bubble isolation, guided bubble release system, and a main fluid flow channel. Bubbles are generated in the side channels where they develop positive pressure. This chamber is connected to a bubble collection channel (air vent) that in turn is connected to a bubble release chamber that is at atmospheric pressure. However, four more potential designs that eventually led to BIRS are also discussed to establish the intended functionality of the BIRS design. In integrated LOC applications, an array of such micropumps could be micromachined with all of them connected to a common bubble release system at atmospheric pressure. If desired, this chamber could contain hydrogel to act as a porous seal as shown in Fig. 1c.

2 Theory

The theoretical basis for the physics of MHD micropumps are now very well understood and have been presented earlier by various researchers (Patel and Kassegne 2007; Hughes et al. 1994, 1995; Ramos et al. 1998; Ramos and Winowich 1990; Winowich and Hughes 1983; Winowich et al. 1987). Recent research works have concentrated on understanding and subsequently mitigating detrimental effects commonly encountered in micropumps. For example, Patel and Kassegne (2007) investigated the influence of electroosmosis and Joule heating on flow rates. Homsy et al. (2005) introduced a mechanism to reduce one of the most challenging aspects of DC-based MHD micropumping, i.e., bubbling. Their work pointed out that DC-based MHD micropumps bubble formation due to electrolysis interferes with the fluid flow necessitating a review of its reaction chemistry to understand its effect on the performance of such micropumps. In this section, we present a theoretical investigation of electrolysis to gain a better understanding of bubble formation and transportation.

Electrolysis of aqueous Sodium Chloride solution, used in these experiments, occurs according to the reduction oxidation equations given in Eqs. 1a–d. According to the standard reduction table, this reaction has a potential of approximately 3 V which corresponds to a current density of 4×10^7 A/m^2 for 2Ω platinum electrodes (100 µm in diameter and 6 mm in length).

Cathode:

$$2H_2O + 2e^- \rightarrow 2OH^- + H_2(g), \quad E^o_{ox} = -0.83 \text{ V} \tag{1a}$$

$$Na^+ + e^- \rightarrow Na, \quad E^o_{ox} = -2.71 \text{ V} \tag{1b}$$

Anode:

$$2Cl^- \rightarrow Cl_2(g) + 2e^-, \quad E^o_{ox} = -1.36 \text{ V} \tag{1c}$$

$$2H_2O \rightarrow O_2(g) + 4H^+ + 4e^-, \quad E^o_{ox} = -1.23 \text{ V} \tag{1d}$$

In practical conditions, reduction does not occur for sodium at the cathode due to higher energy of equilibrium required; instead the sodium stays in the solution in aqueous form as shown in Eq. 2. At the anode, chlorine's concentration is lower than water. Thus oxidation of water is unfavorable even though its reduction potential is similar to chlorine. The overvoltage required to produce oxygen also limits oxygen production. This voltage depends on electrodes/electrolytes chemistry. The overall electrolysis that occurs in aqueous sodium chloride would give off primarily hydrogen and chlorine gas.

$$2NaCl(aq) + 2H_2O(l) \rightarrow 2Na^+(aq) + 2OH^-(aq) + H_2(g) + Cl_2(g) \tag{2}$$

Since, the hydrostatic pressure within the pump is in order of a few Pascals, it does not take many gas molecules to create a gas pocket. Nonetheless, flow should be unaltered if the occlusion's volume is much smaller than the channel's internal volume. Gas bubbles generated by electrolysis will try to reach equilibrium by either escaping to atmosphere or aggregate with other bubbles to reduce their internal pressure. However as more and more bubbles aggregate, internal pressure would eventually burst the bubble aggregate itself. The collapse of the bubble aggregate further propels the fluid along the channel. In an open system, gas bubbles escape to the atmosphere rather than travel along with the fluid and aggregate along the walls due to thermocapillary effects (Kasumi et al. 2000). Since the pump has to be hermetically sealed to prevent contamination for LOC application, a completely open micropump design is not an option.

As a result, the most challenging problem in designing DC MHD micropump is the dispatchment of these air bubbles produced by electrolysis. The coalescence of the bubbles to form larger air pockets which could occupy the entire pump creates synergistically compounding problems. First, the higher internal pressure generated in gas occlusions requires, in turn, a higher pressure head to move them along the channel. Secondly, a Lorentz's force cannot be generated in areas lack of conductive fluid causing a drop in the overall pressure and pumping efficiency.

While it is impossible to prevent the creation of bubbles in high DC currents, it is clear, however, that controlling air bubbles size, rate of accumulation and their location is vital to improving a micropump's performance. This control of bubble sizes and location could be achieved by selecting optimal electrolyte that has the highest reduction oxidation potential injunction with appropriate metal for electrodes. In this research, platinum electrodes and aqueous sodium chloride are selected because they are the most commonly used ones in biological applications. With a better control of bubble location and sizes, the next challenge is to prevent the aggregation of bubbles and enhance their dispersion.

In this research, the reduction and, possibly, the elimination of bubble coalescence is achieved by placing the electrodes in compartments separate from the fluid flow much like what is reported by Homsy et al. (2005). In the approach described by this current research, conduits, placed along the bottom of the walls separating the electrodes and main chambers, serve as both current conductor and bubbles trapping mechanisms. The geometry of these conduits can be altered to vary the electric field distribution and restricting bubbles' entrance to the main pump. Further, this research goes one more step by introducing a guided bubble release system for the dispersion and release of the bubbles whose generation could not be eliminated (Fig. 1b–d).

3 Materials and methods

MHD micropumps are designed using CAD software and machined from polysulfone on a Haas CNC machine (Haas Automation Inc., Oxnard, California). The rapid prototyping offered by CNC is the main motivation for adopting this milling process. In total, five unique MHD designs with increasing sophistication in bubble isolating and discharging capabilities are designed and fabricated. A summary of the configuration and dimensions is given in Table 1. Versions A–C are milled in one unit while Version D and BIRS require milling two parts each that are subsequently epoxy glued. During experiments, the bubble release chamber was not plugged with hydrogel and remained exposed to atmospheric pressure. The experimental set-ups are shown in Fig. 2.

For the experiments involving all the five designs, pump sections are sealed from the external environment by gluing No. 1 glass cover-slips to polysulfone substrate. Custom teflon insulated platinum electrodes (WPI, Saratosa, Florida), 200 μm in diameter and 6.4 mm length (running for the whole length of the main channel) are powered using HP 6236B power supply (Hewlett Packard, Palo Alto, California). The custom electrodes are made by embedding Teflon coated platinum wire inside an epoxy filled 22 gage hypodermic needle. Gold connector is then soldered to the wire at the luer end of the needle for easy connection to power supply. The entire electrode is then coated with paraffin and epoxy to ensure proper insulation leaving only the desired length exposed. To ensure proper placement, electrodes are embedded into the channel using micromanipulator and epoxy glue.

DC current was generated using GoldStar FG-2002C (LG Precision, Seoul, South Korea) function generator coupled with in-house amplifier. Permanent magnets, purchased from Industrial Liquidator (San Diego, California), were used to generate the required magnetic field for micropumps. The magnets have a magnetic flux density of 18 mT. Video recordings are done on Wesco stereoscope (Western Scientific Company Inc., Valencia, California) at 5× magnification using a Zarbeco ZC105 camera (Zarbeco LLC, Randolph, New Jersey). Data analysis is done using Matlab (Mathworks, Natick, Massachusetts).

All experiments are performed using 1 M NaCl solution at 20°C under identical configuration and settings. NaCl solution is equilibrated in micropump for 10 min prior to start of experiments to ensure proper priming with the help of an external pipette. Pumps are activated for 2 min and output volume measured using Pipetman® (Gilson Inc., Middleton, Wisconsin). Air bubbles are monitored and velocities are measured using particle tracking algorithm. Micro-beads of 2 μm size (Polysciences, Warrington, PA) are used for velocity measurement. All measurements were done in triplicates.

To assess the presence and potential magnitude of contribution from electrokinetic flows, control experiments are carried out with electric field only wherein the magnets are removed. Our results show that there was no visible electrokinetic flow in all the micropump designs considered here under the application of electric field. The rather large size of the channels (800 μm × 800 μm) is believed to actually minimize the effect of electroosmotic flow as demonstrated by Patel and Kassegne (2007).

4 Results and discussion

A. Conventional Single Channel/Compartment Micropump: to demonstrate the feasibility of CNC MHD micropump and the effect of unmitigated bubble formation and transport on pumping, and more specifically on flow rate, a simple conventional MHD pump with electrodes along the side walls is machined and tested. In this configuration, flow rates of 100 and 200 μl/min are obtained for 5 and 20 V, respectively (cf. Fig. 3, Table 1). These results show that the flow rate is not linearly proportional to the voltage as

Table 1 Summary of the five versions of bubble isolating and discharging MHD micropump designs

Design	Front View	Top View	Isometric View	Comments
A	d	Main channel	w	Traditional design with electrodes along sidewalls.
B	d	Electrode chamber Main channel	3w	Modified with electrode compartments. Microfringes are 200 μm x 400 μm.
C	2d	Main channel	3w	Modified with electrode compartments and raised main channel. Shaded part is solid.
D	2d	250 μm ϕ perforations	3w	Modified with electrode compartments and raised main channel and perforations for electrical continuity
E	1.5d slit	Current conformer Main channel	3w	Modified with electrode compartments and spacers for gas escape. Release chamber not shown for clarity.

Note that all the drawings are to scale. Electrodes are noted as darkly shaded region. All main channels have a size of 800 μm × 800 μm. Length of pumping section = 6.4 mm. Version A—Conventional single channel/compartment micropump, version B—Compartmentalized micropump, version C—Compartmentalized micropump with elevated main channel, version D—Compartmentalized micropump with buried electrodes, version E—BIRS micropump. $d = 800$ μm, $w = 800$ μm

expected. The chaotic and rapid bubbles generation as well as the unpredictable dispersion at 20 V is considered to be the main reason for such major drop off in observed flow rate. Other phenomena such as Joule heating and electroosmotic flow, observed by other researchers, are considered additional potential

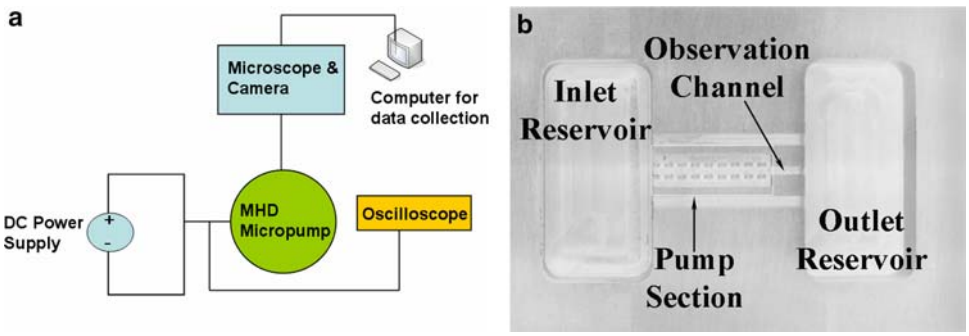

Fig. 2 Experimental set-up. **a** Schematics of the experimental set-up consisting of power supply, micropump, microscope and camera as well as data acquisition. **b** Location of inlet and outlet reservoirs, pump section and the observation channel. Here, the pump sections are sealed from the external through glass cover-slips. Custom teflon insulated platinum electrodes 200 μm in diameter are powered using HP 6236B power supply. AC current is generated using GoldStar FG-2002C function generator coupled with in-house amplifier. Permanent magnets are used to generate the required magnetic field for micropumps. A video recording is done on Wesco stereoscope at ×5 magnification using a Zarbeco ZC105 camera. Data analysis is done using Matlab

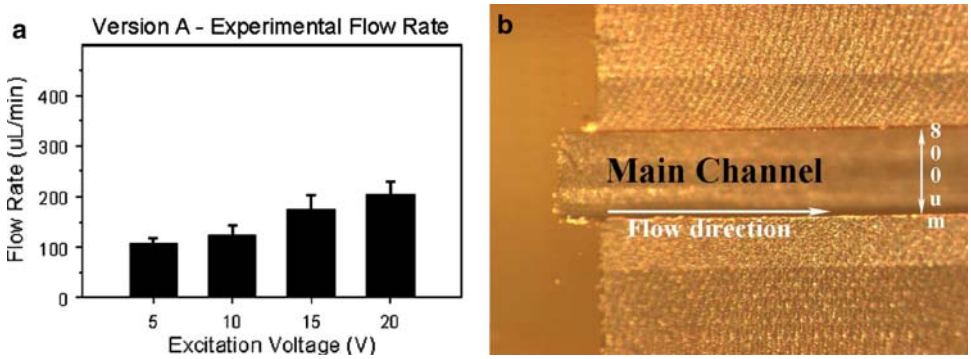

Fig. 3 **a** Flow rate of single channel micropump MHD (version A) under DC excitation; **b** micrograph of the same MHD micropump

sources of this nonlinear behavior. Large air pockets tend to accumulate near the entrance of the channel mainly due to the significant amount of electrolytes available at that location. Even at lower voltages, uncontrolled bubbles aggregation is observed with a potential to abruptly choke large sections within the pump of liquid and deactivate the pump. Further, gases produced near the inlet are observed to escape towards the entrance due to the short distance along with a pressure drop in the direction of the entrance. In general, this design suffers from excessive bubbling limiting its usefulness in high-current and—therefore—high flow rate applications.

B. Compartmentalized Micropump: in the second design, electrodes compartments and evenly spaced microfringes of 200 μm width and 400 μm length that run through the height of the main channel are introduced to isolate the gas bubbles from entering the flow cell. These microfringes are spaced at 400 μm center to center. Flow rates of 150 and 300 μl/min are observed at 5 and 20 V, respectively (cf. Fig. 4, Table 1). Bubbles coalescence and aggregation in the main channel continue to be a problem. Initially, small bubbles flow into the main channel and toward the exit. However some of these bubbles are observed to accumulate around the walls of the microfringes as well. As more bubbles aggregate, the occlusions begin to grow. Eventually, they disrupt the current continuity in the main channel, hence disabling the pump. This suggests that the microfringes alone by themselves are not effective in mitigating the adverse effects of bubbles on flow.

C. Compartmentalized Micropump with Elevated Main Channel: in this configuration, in addition to the three compartments for the main channel and the side channels, elevation is provided for the main channel to further separate the electrodes from the main channel so that bubbles do not travel sideways to the main channel (cf. Fig. 5, Table 1). The depth of the main channel remains at 800 μm. Electrolysis only occurs at the electrode interfaces. Gas bubbles rise out of fluid to the surface where there is less pressure. Having an open pump is the easiest solution to the bubble interference problem. By increasing the depth of the electrodes' compartments, the third design further separates the electrodes to reduce the aggregation of bubbles. In this design, it is found out that the elevation of the main flow channel has a significant impact on the pump's output by mitigating the effect of bubbles. More bubbles are attracted along the walls of the electrodes compartments than the edges of microfringes. The flow rates seem to scale linearly with the voltage. Flow rates of 150 and 400 μl/min were observed at 5 and 20 V, respectively (see Fig. 5a).

D. Compartmentalized Micropump with Buried Electrodes: the fourth design contains—in addition to side channels—a perforated layer that isolates the

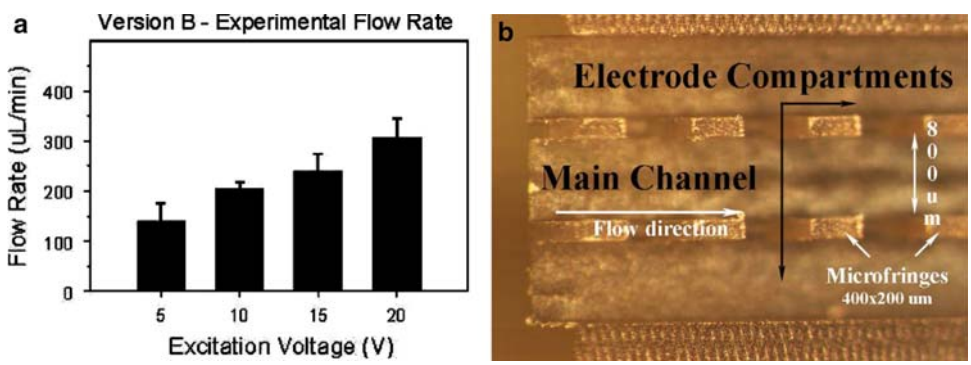

Fig. 4 **a** Flow rate of compartmentalized micropump MHD pump (version B) under DC excitation; **b** micrograph of compartmentalized micropump MHD. Main channel, microfringes (200 μm × 400 μm), inlet reservoir, and electrode compartments are shown

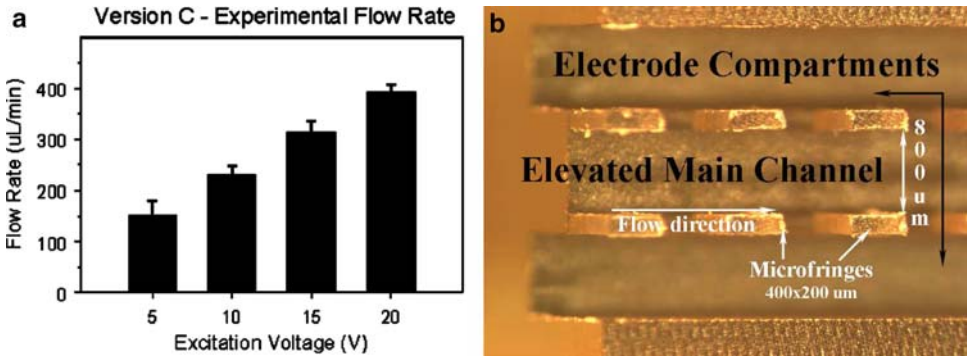

Fig. 5 **a** Flow rate of compartmentalized MHD micropump with elevated channel (ver03) under DC excitation; **b** micrograph of the MHD micropump. Elevated main channel, microfringes (200 μm × 400 μm), inlet reservoir, and electrode compartments are shown

electrolyzed bubbles from entering the main pump channels while maintaining electrical conduction as shown in Fig. 6 and Table 1. Essentially, this design is similar to version C (compartmentalized micropump with elevated main channel) except that there is a physical separation layer that contains 250 μm diameter perforation holes. The intent of introducing the perforations is to arrest the transport of bubbles to the main channel. There are four possible electrodes placement configurations possible. With the anode in the bottom electrode chamber and cathode on the upper layer, a flow rate of 75 and 325 μl/min were observed for 5 and 20 V excitation, respectively. For this design, this electrodes configuration gives the best results. The reason is that chlorine gas, produced at the anode and slightly soluble in water, has an opportunity to equilibrate with the surrounding and travel with the liquid toward the exit without impeding flow. Meanwhile the more volatile and rapid forming hydrogen can escape to the atmosphere faster since they are in the upper layer. As expected, alternating the anode and cathode location resulted in flow rate of 50 and 200 μl/min.

E. BIRS Micropump: in this design that forms the main contribution of this research, instead of microfringes, current continuity is achieved through open channels at the bottom layer that connect the electrode compartments and the main pumping channel (cf. Fig. 7, Table 1). As seen by the other four previous designs discussed here, microfringes are demonstrated to actually promote bubble coalescing. As a result, they are replaced with a solid connecting wall (that divides the main channel from the electrode channels) with a slit at the bottom to allow ionic fluid continuity.

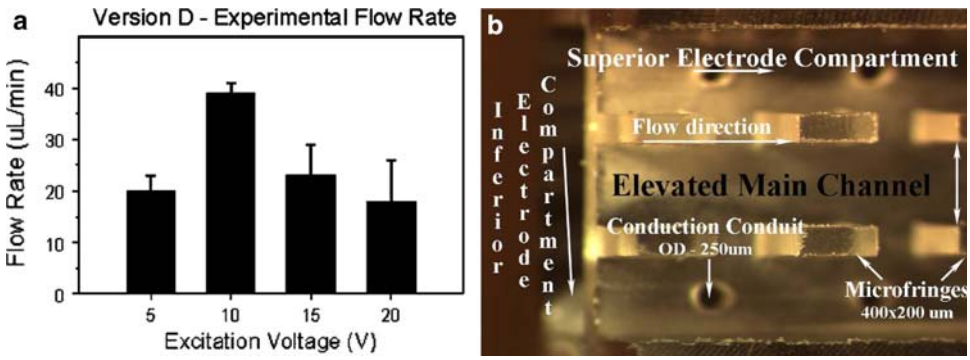

Fig. 6 **a** Flow rate of compartmentalized MHD micropump with buried electrodes (version D) under DC excitation; **b** micrograph of the same MHD micropump. Perforated layers, microfringes, inlet reservoir, and electrode compartments are shown

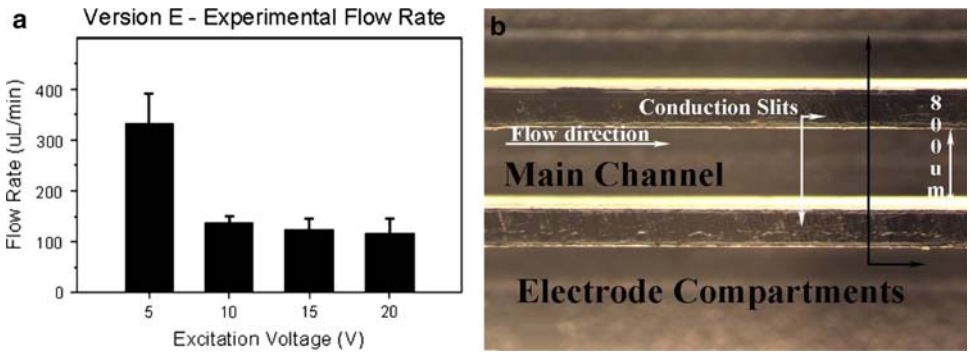

Fig. 7 **a** Flow rate of the BIRS MHD micropump (version E) under DC excitation; **b** micrograph of BIRS MHD micropump. Main channel and electrode compartments are shown

With this slit configuration, current density can be manipulated by adjusting the height of the connecting wall. The main objective of this design is to have free dead space above the electrode compartments allowing for electrolyzed gas to escape. This free space above the electrode compartments allows electrolyzed gas to escape to the atmosphere through the bubble collection channel and bubble release chamber as shown in Fig. 1. Electrolyzed air pockets accumulate along the walls of the barriers instead of aggregating along the fringes, then float to the bubble collection chamber and subsequently to the bubble release chamber from where they are discharged at atmospheric pressure. In the BIRS micropump, crossing channels are completely removed and replaced by a solid barrier.

This design gives the best result at the lowest voltage setting. Maximum flow rate of 330 μl/min is observed at 5 V. In version D (Compartmentalized micropump with buried electrodes), 20 V is required to achieve flow rate comparable to this. However, as the voltage is increased, the efficiency of the BIRS MHD micropump decreases because more bubbles are generated than that can be handled in the bubble trapping and isolation region. These bubbles, then, coalesce and impede the fluid flow as in the other conventional designs. A possible remedy is to increase the size of the bubble isolation chamber shown in Fig. 1b–d.

4.1 Simulation results

Numerical models are built using FEA program (COMSOL FEMLAB FEA Software 2005) to predict the electrical and magnetic field distributions, Lorentz force distributions and magnitudes, and flow rates for each of the five designs. The numerical models do not include the effects of bubbles and assume a simple one-phase flow. A two-phase flow model—which is beyond the scope of the current work—is required to model bubble generation and propagation. Detailed discussion of the numerical models for MHD micropumps applicable to this research is provided in Patel and Kassegne (2007). From the models, we predict the total Lorentz's force in the channel and subsequently the flow rates. NaCl solution of 1 M strength and conductivity of 1.5 S/m is used. A magnetic flux density of 18 mT is considered.

A summary of the maximum theoretically predicted velocities as well as Lorentz force intensities is given in Table 2. Further, Fig. 8 summarizes a comparison of theoretically predicted velocity profiles in the various MHD pump configurations along the pump's height at entrance and along the length of pump at center. With regard to velocity considerations alone, the conventional single channel design exhibits the highest performance followed by version D design (compartmentalized micropump with buried electrodes). As summarized in Table 2, based on theoretical predictions, the single channel design of size 800 μm × 800 μm has the highest velocity and hence flow rate; however, the model does not include the effect of bubbles. The high theoretical flow rate is due to high current density and, hence, high Lorentz's Force achieved by the closer spacing of the electrodes as shown in Table 2. The table further shows that the Lorentz's Force for Version A is the highest followed by that of Version B and then BIRS design. Consequently, the compartmentalized channel design (version B) has the second highest predicted flow velocity. The BIRS design has the next highest theoretical flow velocity with no consideration of the effect of bubbles. As expected, the FEA simulations show that with no consideration of bubble effect, the flow velocity is a function of just the geometry and electrode spacing. However, looking further, the distribution of the flow velocity summarized in the table offer interesting insight into the spatial distribution of the velocity field. The compartmentalized micropump design (version B) and BIRS seem to have an ideal flow velocity distribution with the flow field concentrated in the main pump channels. The BIRS design seem to exhibit some side bleeding of the flow velocity which tends to increase with increased depth of separation (slit) of the side wall. The design with compartmentalized micropump with elevated main channel (version C) and compartmentalized micropump with buried electrode (version D) exhibit quite a significant amount of flow in the side channels. Further, the version D MHD micropump seems to have a significant flow at the bottom electrode channel—at a location where it is wasted.

For BIRS as well as the other four designs, the theoretical values of flow rates determined by FEA are then compared with those obtained by experimental measurements as shown in Fig. 9. The comparison of flow rates for 5 V between experimental and FEA results shows a relatively closer agreement varying from a difference of 25% for BIRS design to about 300% for version A (i.e., Conventional single channel/compartment micropump). As the amount of bubbles is relatively smaller at 5 V, the flow rates are not expected to be drastically affected by bubbles; hence the acceptably close agreements in most of these designs. However, as the voltage increases to 10, 15, and then 20 V, the experimentally measured flow rates assume a value as low as 10% of the theoretically predicted flow rates. Figure 10 shows the variation of the difference between theoretical and experimental results as a function of voltage. In general, the trend indicates that the conventional single chamber MHD micropump (i.e., version A) has the highest discrepancy (or lowest

Table 2 Summary of theoretically predicted maximum velocities and Lorentz forces in the various MHD micropumps considered in this research

Design Type	Velocity Profile (Elevation)	Velocity Profile (Top View)	Max. Lorentz Force (N/m^2)	Maximum Velocity (mm/s)
A – Conventional single channel/compartment micropump	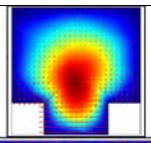	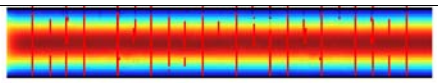	1.27	7.11
B - Compartmentalized micropump	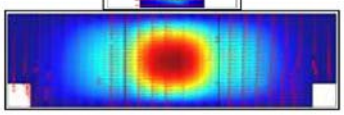	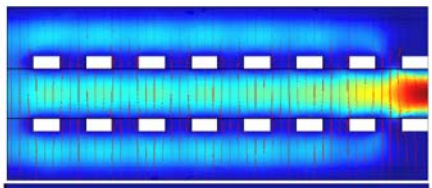	0.47	3.62
C - Compartmentalized micropump with Elevated Main Channel:	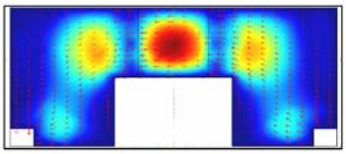	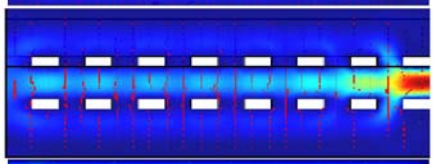	0.37	1.011
D - Compartmentalized micropump with Buried Electrodes:	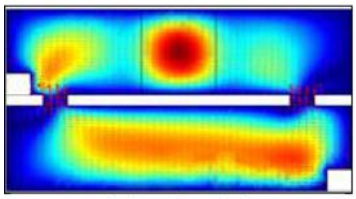	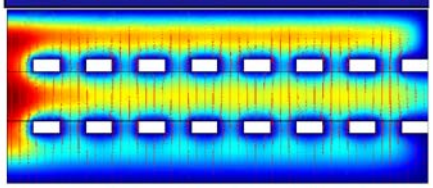	0.18	1.858
E - BIRS micropump	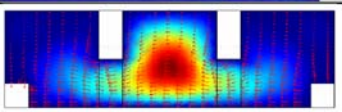	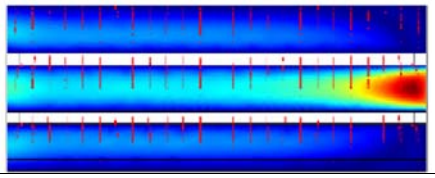	0.43	2.196

efficiency). The introduction of bubble coalescence retardation mechanisms in designs B–E, in general, tends to improve the efficiencies with the BIRS design having the best comparison.

The BIRS MHD micropump seems to degrade in performance as measured by its flow rate when higher voltages are used. As explained before, this is due to the generation of excessive amount of bubble that cannot be handled in the bubble trapping and isolation region. These bubbles that coalesce tend to seriously impede the fluid flow as in the other conventional designs. However, it needs to be noted that a flow rate of 300 μl/min for the main channel cross-section of 800 μm × 800 μm is considered quite high for an operating voltage of 5 V; therefore there is no pressing need for increasing the voltage to higher values.

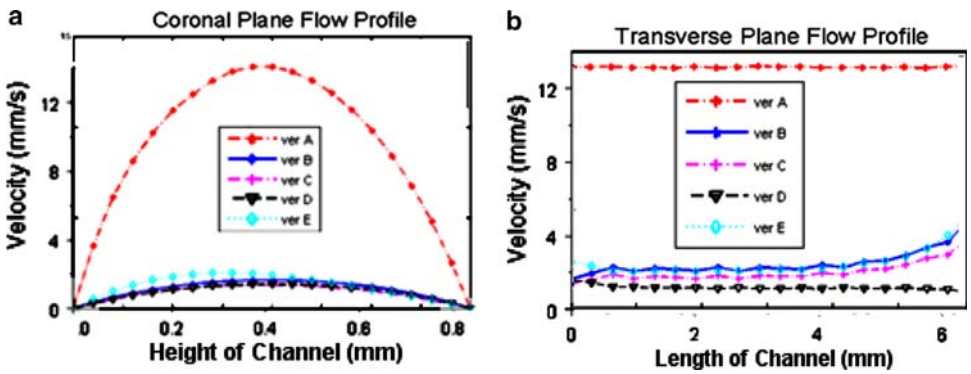

Fig. 8 Comparison of theoretically predicted velocity profiles in the various MHD pump configurations. **a** Along pump's height at entrance. **b** Along length of pump at center

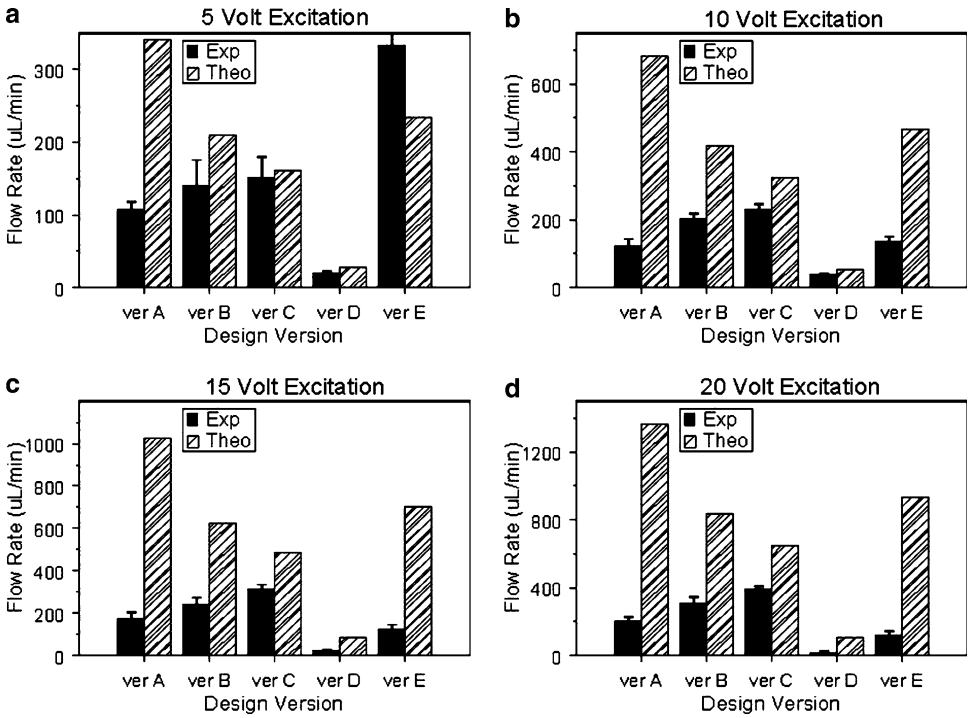

Fig. 9 Comparison between theoretically predicted and experimental flow rates in the various MHD pump configurations. **a** 5 V, **b** 10 V, **c** 15 V, **d** 20 V

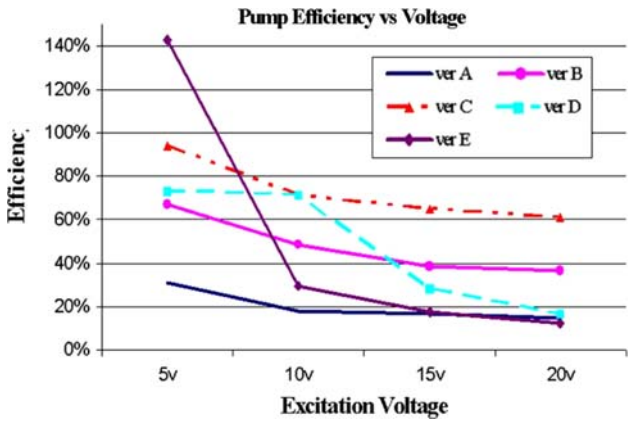

Fig. 10 Comparison of micropump efficiency between theoretically predicted and experimental flow rates in the various MHD pump configurations. **a** 5 V, **b** 10 V, **c** 15 V, **d** 20 V. The efficiency of a given design is given as (1.0 − (theoretical value − experimental value)/theoretical value) × 100.0

5 Conclusions

In this research, we report a novel high current density and high flow rate DC-based MHD micropump with a bubble isolation and release system. Gas bubbles, particularly, hydrogen generated by high current density at the electrodes are the main culprit in low experimental flow rate compared with theoretical values. These tiny bubbles coalesce in the flow channel thus obstructing the flow of fluid. Since hydrolysis is inevitable with DC excitation, compartmentalized electrode channels with bubble isolating and coalescence retarding mechanisms and bubble release systems are implemented to prevent the coalescence of these bubbles. The micropump introduced here called BIRS is demonstrated to be capable of generating a flow rate of up to 325 μl/min using 1 M NaCl solution in DC mode with potentials of 5 V and current density of about 5,000 A/m^2 for a main channel of 800 μm × 800 μm cross-section and 6.4 mm length. The performance of the pump is shown to be exceptionally well at low voltages (5 V); but degrades at higher voltages due to excessive bubbling that requires larger bubble release chambers.

The results from experiments were compared with FEA simulations which demonstrated that the numerical models offer interesting and useful insight into the spatial distribution of the velocity field as determined by the Lorentz's force. However, the quantitative agreement between experiments and FEA show variations between a low of 25% to a maximum of 300%. These variations are due to the one-phase flow assumptions in the FEA model. Modeling of the generation and propagation of bubbles through a two-phase flow approach is currently being pursued as extension of this work to improve the agreement between theoretical and experimental approaches.

In general, since one of the main requirements for micropumps to be used in fully automated Lab-on-a-chip (LOC) applications is the generation of flow rate in the range of 100 μl/min or more, the BIRS design promises to be a suitable choice to meet this requirement. Further, the ability to machine a series of these micropumps in an array

format where the BIRS pumps share a common bubble release chamber could offer an efficient micropumping system applicable to a variety of LOC and microTAS systems under low voltage conditions.

References

Alfven H (1942) Existence of electromagnetic—hydrodynamic waves. Nature 150:405

Bao JB, Harrison DJ (2003) Fabrication of microchips for running liquid chromatography by magnetohydrodynamic flow. In: Proceedings of the 7th international conference on miniaturized chemical and biochemical analysts systems, Squaw Valley, California, USA

Bendib S, Français O (1999) Analytical study of microchannel and passive microvalve application to micropump simulator. In: Proceedings of the SPIE, pp 200–208

FEMLAB FEA Software (2005) Reference Manual, version 3.1, COMSOL Inc

Heng KH, Huang L, Wang W, Murphy MC (1999) Development of a diffuser/nozzle type micro-ump based on magnetohydrodynamic (MHD) principle. Proc SPIE—Microfluidic Dev Syst II 3877:66–73

Heng KH, Wang W, Murphy MC, Lian K (2000) UV-LIGA microfabrication and test of an ac-type micro-pump based on the magnetohydrodynamic (MHD) principle. Proc SPIE—Microfluidic Dev Syst III 4177:174–184

Heschel M, Mullenborn M, Bouwstr S (1997) Fabrication and characterization of truly 3-D diffuser/nozzle microstructures in silicon. J Microelectromech Syst 6(1):41–47

Homsy A, Koster S, Eijkel JCT, Berg A, Lucklum F, Verpoorte E, de Rooij NF (2005) A high current density DC magnetohydrodynamic (MHD) micropump. Lab Chip 5(4):466–471

Huang L, Wang W, Murphy MC (1999) A lumped-parameter model for a micro-pump based on the magnetohydrodynamic (MHD) principle. Proc SPIE–Des Test Microfabric MEMS MOEMS 3680:379–387

Huang L, Wang W, Murphy MC, Lian K, Ling ZG (2000) LIGA fabrication and test of a DC type magneto-hydrodynamic (MHD) micro-pump. Microsyst Technol 6:235–240

Hughes M, Pericleous KA, Cross M (1994) The CFD analysis of simple parabolic and elliptic MHD flows. Appl Math Model 18:150–155

Hughes M, Pericleous KA, Cross M (1995) The numerical modeling of DC electromagnetic pump and brake flow. Appl Math Model 19:713–723

Jang J, Lee SS (2000) Theoretical and experimental study of MHD micro-pump. Sens Actuators A 80:84–89

Jeong OC, Yang SS (2000) Fabrication and test of a thermo-pneumatic micro-pump with a corrugated p+ diaphragm. Sens Actuators A 83:249–255

Kasumi H, Solomentsev YE, Guelcher SA, Anderson JL, Sides PJ (2000) Thermocapillary flow and aggregation of bubbles on a solid wall. J Colloid Interface Sci 232:111–120

Lemoff AV, Lee AP (2000) An AC magnetohydrodynamic micro-pump. Sens Actuators B 63:178–185

Patel V, Kassegne SK (2007) Electroosmosis and thermal effects in magnetohydrodynamic (MHD) micropumps using 3D MHD equations. J Sens Actuators B 122:42–52

Ramos A, Morgan H, Green NG, Castellanos A (1998) AC electronics: a review of forces in microelectrode structures. J Phys D: Appl Phys 31:2338–2353

Ramos JI, Winowich NS (1990) Finite difference and finite element methods for MHD flows. Int J Numer Methods Fluids 11:907–934

Strachan JD, Bitter M et al (1987) High-temperature plasmas in a tokamak fusion test reactor. Phys Rev Lett 58:1004–1007

Sutton GW, Sherman A (1965) Engineering magnetohydrodynamics. McGraw-Hill Book Company, New York

Wang PJ, Chang CY, Chang ML (2004) Simulation of two-dimensional fully developed laminar flow for a magneto-hydrodynamic (MHD) pump. Biosens Bioelectron 20:115–121

Winowich NS, Hughes WF (1983) A finite element analysis of two-dimensional MHD flow. AIAA Prog Astronaut Aeronaut 84:313

Winowich NS, Hughes WF, Ramos JI (1987) Numerical simulation of electromagnetic pump flow. Numer Methods Laminar Turbulent Flow 5(2):1228–1240